Modelling the response of mangroves and saltmarshes to sea-level rise: model development and validation

Kerrylee Rogers[1], Laura A. Mogensen[2], Oxana Repina[3] and Neil Saintilan[4]

[1]School of Earth, Atmospheric and Life Sciences, University of Wollongong, Wollongong, NSW, 2522, Australia.

[2]School of Earth, Atmospheric and Life Sciences, University of Wollongong, Wollongong, NSW, 2522, Australia.

[3]School of Earth, Atmospheric and Life Sciences, University of Wollongong, Wollongong, NSW, 2522, Australia.

[4]School of Natural Sciences, Macquarie University, Sydney, NSW, 2109, Australia.

Corresponding author: Kerrylee Rogers (kerrylee@uow.edu.au)

Key Points:

- Models of the response of coastal wetlands to sea-level rise are needed to inform coastal planning and decision making
- Poorly calibrated and insufficiently validated models reduces confidence in model outputs and suitability for informing decisions
- Model testing undertaken across three timescales provided confidence to use model projections over timescales suitable for planning

Abstract

Models of the response of mangrove forests and saltmarshes to sea-level rise are needed to inform coastal decision making. Zero-dimensional models that simulate evolution of a point are foundational for developing spatially explicit landscape models projecting coastal wetland extents under future sea-level rise scenarios. However, both zero-dimensional and spatially explicit landscape models have suffered from insufficient calibration and inadequate validation. In this study, a zero-dimensional model framework was parameterised using real data from four sub-sites exhibiting varying rates of mineral and organic matter addition and autocompaction. The model was calibrated to correspond to tidal parameters at each sub-site and validation was undertaken across three timescales to assess model efficacy. Short-term validation encompassed the period over which measurements of surface elevation gain were determined using a network of surface elevation tables (~20 years); medium-term validation encompassed the period when higher resolution colour aerial photography was available (~35 years); and long-term validation focussed on the period of landscape evolution occurring since the mid-Holocene. The model performed well at the medium to long-term scale and was within the range of variability arising from surface elevation table measurements. This study demonstrates the critical need for site-specific data, a crucial component that is undervalued, often insufficiently resourced to generate useful data, and commonly addressed by extrapolating parameters generated from elsewhere. Validation has provided the necessary confidence for further model development at the landscape scale that will account for processes operating both vertically and laterally, such as shoreline erosion and tidal creek extension.

Plain Language Summary

The fate of coastal wetlands is a key concern for coastal managers as sea level is projected to rise and modify the position and arrangement of coastal wetlands. Managers require more information about how coastal wetlands adjust to sea-level rise, and the implications this will have on adjoining land-use, nearby infrastructure and the supply of ecosystem services, such as wildlife habitat, coastal protection and carbon storage. Models of the response of mangroves and saltmarshes to sea-level rise assist with planning and decision making, but often are not calibrated with site-specific or real-world data, or may be insufficiently tested to confirm their usefulness. Here we use a model describing processes contributing to coastal wetland adjustment to sea-level rise and apply real-world data to the model. This allowed for simulations to be compared against real-world conditions to asses the model performance. The model was tested over three projection periods, ranging from decades to millenia. Comparisons provided confidence to use the model for planning and decision making, and the model is being prepared for generating maps of coastal wetlands on the basis of a range of future scenarios.

1 Introduction

Coastal wetlands comprising of mangrove forests and saltmarshes occupy a unique niche within the upper half of the tidal frame; a niche that is projected to increase its elevation as sea level rises (*Schuerch et al.*, 2018). Coastal wetlands can adapt to this changing tidal frame by accumulating mineral and organic material in substrates to increase substrate elevations, and by translating laterally to higher elevations (*Fagherazzi et al.*, 2020; *Woodroffe et al.*, 2016). There is, however, evidence from early Holocene paleo-stratigraphic observations that the capacity of coastal wetlands to adapt in situ to sea-level rise may become highly unlikely as rates of sea-level rise exceed approximately 7 mm $^{yr-1}$ (*B P Horton et al.*, 2018; *N Saintilan et al.*, 2020).

Based on current likely projections, this rate of sea-level rise will likely be exceeded by 2080-2100 when warming exceeds 3°C (*Fox-Kemper et al.*, 2021). This means that lateral space for coastal wetlands to extend to higher elevations will become increasingly important to maintain and enhance the ecosystem services provided by coastal wetlands (*Nicholls*, 2011). These services are substantial, will improve the resilience of shorelines to climate change and may contribute to climate mitigation efforts by enhancing carbon sequestration (*Barbier et al.*, 2011; *Sutton-Grier et al.*, 2014). However, the coast is a highly contested space and, in many locations, lateral space for migration is limited by barriers to tidal exchange (e.g. sea walls, roads and buildings), or conflicting land use and land cover (*Doody*, 2004; *Pontee*, 2013; *Torio and Chmura*, 2013). As a consequence, there is increasing need to plan for coastal wetland adaptation to sea-level rise, with models of coastal wetland evolution being necessary to provide the required confidence in projections that are used to inform planning decisions (*Wiberg et al.*, 2020).

Zero-dimensional (0D) models of substrate evolution are used to explore future coastal wetlands scenarios on the basis of change in elevation of a single point (*Fagherazzi et al.*, 2012), and are the basis for one-dimensional models of changes along a transect and fully three-dimensional models that can be presented as maps of projected coastal wetland distribution. These models are all useful for planning, however, there is an increasing desire for high precision maps of projected distribution changes to inform planning and decision making at the local scale. There are a range of models that have been developed to project coastal wetland responses to sea-level rise, largely arising from research undertaken in the USA and Europe (*Fagherazzi et al.*, 2012; *Fagherazzi et al.*, 2020; *Wiberg et al.*, 2020), and rarely from locations in the southern hemisphere (*Oliver et al.*, 2012; *Rodríguez et al.*, 2017; *Sandi et al.*, 2021). This is problematic as the sea-level history of coastal wetlands in the southern hemisphere, which has been relatively stable for the past few millennia, contrasts that of the northern hemisphere where shorelines have been highly influenced by glacio-isostatic adjustment (*Clark and Lingle*, 1979; *Khan et al.*, 2015). Sea-level history has important implications for coastal wetland evolution (*Rogers et al.*, 2019a), and substrate carbon content and bulk density (*Rogers and Saintilan*, 2021; *Rogers et al.*, 2022; *Neil Saintilan et al.*, 2022). In addition, the vegetation composition of coastal wetlands can be remarkably different. For example, mangrove forests generally extend to higher latitudes in the southern hemisphere due to the modifying effect of expansive oceans on coastal temperatures, and the improved tolerance of the mangrove species *Avicennia marina* to lower temperatures (*Quisthoudt et al.*, 2012; *N. Saintilan et al.*, 2014). In addition, saltmarsh diversity can be high, particularly where *Spartina* species are absent (*Adam*, 2009; *Neil Saintilan*, 2009), and the outcome of high species diversity can be complex arrangements of mangrove and saltmarsh species within the upper half of the tidal frame (*Bridgewater and Cresswell*, 1999). Models of coastal wetland response to sea-level rise that have been developed in the northern hemisphere may, therefore, not be effective in the southern hemisphere, and validation is necessary to ensure their efficacy. Furthermore, models should be calibrated using data from the southern hemisphere to account for species-specific influences on organic matter addition to substrates, rather than extrapolating the response of coastal wetlands to conditions beyond their geographic range. Unfortunately, both calibration with local data and validation of models to local conditions is rarely undertaken when modelling the response of coastal wetlands to sea-level rise.

Many 0D models of marsh evolution build upon the framework proposed by *Allen* (2000) that accounts for the changing tidal position of coastal wetlands in response to mineral and organic matter addition to substrates, autocompaction of substrates and sea-level rise; with glacio-isostatic adjustment, subsidence or uplift being accounted for when occurring at a site. Mineral addition is typically included using a linear relationship with inundation frequency, and often calibrated according to a dimensionless measure of tidal position (*Wiberg et al.*, 2020). Following the findings of Morris et al. (2002), organic matter addition is commonly incorporated according to a quadratic relationship, with the premise being that organic addition will be greatest at the mid-point between the vertical distribution of vegetation. Autocompaction is evidently a more complex measure to incorporate, and many studies either presume autocompaction operates solely via decomposition of organic material (*Zhang et al.*, 2020), or apply a consistent autocompaction factor across the tidal frame (*Marani et al.*, 2013), despite considerable evidence that autocompaction is spatially variable, asymptotically limited (*Allen*, 2000) and related to vertical accretion (*Rogers and Saintilan*, 2021; *Neil Saintilan et al.*, 2022). There are some exceptions to these treatments of autocompaction that incorporate sub-models addressing the various aspects leading to autocompaction, including decomposition of organic material, compression and consolidation (*Mudd et al.*, 2009; *Swanson et al.*, 2014; *Thorne et al.*, 2018).

In this study we seek to address some of the deficiencies in previous modelling exercises by parameterising and calibrating the *Allen* (2000) model according to conditions observed at a study site in the southern hemisphere where sufficient data is available for model development: Westernport Bay, Victoria (*Rogers and Saintilan*, 2021; *Rogers et al.*, 2022). This study builds upon an extensive period of data collection that has provided the basis for calibrating sub-models of mineral and organic matter addition and autocompaction of substrates using real data from co-occurring mangrove forests and saltmarshes. Modelling co-occurring mangrove and saltmarsh forests has rarely been undertaken (*Oliver et al.*, 2012), and adds more complexity to the modelling framework than is typically presented for saltmarsh or mangrove models alone. In addition, the model is calibrated for a range of sub-sites that represent conditions of varying sediment supply. These sub-models were parameterised with unique datasets: a 20-year record of surface elevation gain and vertical accretion from a network of surface elevation tables coupled with marker horizons (SET-MH); detailed analyses of sedimentation over the past 50-150 years from radiometric analyses; organic matter concentrations within substrates; and inundation characteristics (*Rogers and Saintilan*, 2021; *Rogers et al.*, 2022). Following calibration, validation was undertaken and targeted three timescales: short-term validation encompassed the observational period of SET-MH measurements; medium-term validation encompassed the period when higher resolution colour aerial photography was available (35-years); and long-term validation focussed on the period of landscape evolution occurring under relatively stable sea levels since the mid-Holocene. This degree of temporal validation also addresses concerns regarding timescale bias in assessments of vertical change in coastal wetlands (*Breithaupt et al.*, 2018). It is anticipated that this model can be used to explore future sea-level rise scenarios over a range of management-relevant timescales, incorporating processes influencing landscape evolution and with further modification, applied in three dimensions to map projected shoreline changes under future sea-level rise scenarios.

2 Materials and Methods

2.1 Study area

Model development, calibration and validation was undertaken using data collected in coastal wetlands of Westernport Bay, Victoria, Australia, over a 20 year measurement period (*Rogers and Saintilan*, 2021; *Rogers et al.*, 2022). Mangrove forests comprising the low temperature tolerant *Avicennia marina* and highly diverse saltmarshes occupy the upper half of the tidal frame, whilst seagrass beds occupy low energy tidal flats in the lower half of the tidal frame (*Boon et al.*, 2015).

Westernport Bay is a large marine embayment (~680 km^2) that drains a catchment of 3433 km^2 (Figure 1). The region is relatively tectonically and isostatically stable, as evident from negligible vertical land movement recorded on tide gauges (*Khan et al.*, 2015; *White et al.*, 2014). Post-glacial sea levels increased to near present levels at approximately 7 ka, and debate continues regarding the occurrence of a highstand of 1-1.5 m above present levels (*Dougherty et al.*, 2019; *Kennedy et al.*, 2020; *Lewis et al.*, 2013; *Sloss et al.*, 2007). A tide gauge is located at Stony Point and indicates a linear trend of increasing mean sea level in the order of 3.0 ± 0.4 mm yr^{-1} between 1981 and 2017 (*Rogers and Saintilan*, 2021).

Service Layer Credits: Source: Esri, Maxar, Earthstar Geographics, and the GIS User Community

Figure 1. Study location at Westernport Bay, Victoria, Australia, and sub-sites used for model parameterisation, including French Island, Kooweerup, Quail Island and Rhyll Inlet.

Westernport Bay has two entrances to Bass Strait with the eastern entrance exhibiting more constricted tidal movement than the western entrance. Tides propagate clockwise through the western entrance, and anticlockwise through the eastern entrance, converging along the northeastern portion of the embayment. The tidal regime is semi diurnal and has a range of up to 3.1 m, and significant tidal amplification is evident along the Upper North Arm (*Water Technology*, 2014). The embayment is relatively shallow and sediment is largely yielded from hillslope, gully and riverbank erosion occurring in sub-catchments located on the north-eastern shoreline of Westernport Bay, namely the Lang Lang River (0.47 t ha^{-1} yr^{-1}), Bass River (0.30 t ha^{-1} yr^{-1}), Bunyip River (0.25 t ha^{-1} yr^{-1}), and to a lesser degree Yallock Creek (0.21 t ha^{-1} yr^{-1}) and Cardinia Creek (0.15 t ha^{-1} yr^{-1}) (*Hughes et al.*, 2003). Despite substantial sediment yield, considerable cliff erosion occurs in the same vicinity as these sediment sources and largely occurs in response to fetch-based waves that propagate normal to the north-eastern shoreline (*Water Technology*, 2014).

This study specifically uses data collected from four sub-sites in Westernport Bay, French Island, Kooweerup, Quail Island and Rhyll Inlet (Figure 1). A network of SET-MH was established at these sub-sites in October 2000 to provide information on rates of vertical accretion, surface elevation gain and autocompaction; these results have been reported in *Rogers and Saintilan* (2021). Cores were also extracted at each sub-site to characterise organic matter within substrates and develop a sediment chronology using ^{210}Pb dating techniques, with results being reported in *Rogers et al.* (2022). These studies demonstrate that rates of sedimentation and vertical elevation gain are highest at study sites along the Northern Arm where tidal flat development is substantial and fetch based wave activity operates parallel to the shoreline. Sediment addition was found to be lower within the smaller tidal creek system of Rhyll Inlet, and lowest on the eastern shoreline of Quail Island where hydrodynamic energy and limited accommodation space restricts coastal wetland development.

2.2 Model description

The model developed for this study applied the 0D model proposed by (*Allen*, 2000) that underpins other parameterised models of coastal wetland response to sea-level rise, including WARMER (*Swanson et al.*, 2014; *Thorne et al.*, 2018) and OIMAS-N (*Mudd et al.*, 2009). The model was parameterised with data available for the study site. This included data on rates of mineral and organic matter addition within substrates, and autocompaction, which were placed in the context of a tidal frame influenced by sea-level rise (Eq 1). For simplicity, the tidal frame was presumed to remain stable, despite emerging evidence that the tidal frame can be modified by geomorphological changes to coasts in response to sea-level rise, and other activities, such as dredging (*Khojasteh et al.*, 2021). Mineral matter addition was also presumed to be delimited by tides, as occurs in many locations where terrigenous inputs through overland flow or aeolian processes are limited. As the primary vegetation zones are vertically distributed between approximately mean sea level and the limits of tidal inundation, organic matter addition was also constrained to these boundaries.

Accordingly, incremental elevation change (E_{t+1}) was parameterised as per Equation 1:

$$E_{t+1} = E_t + MAR_{E(t)} + OAR_{E(t)} - AC_t - SLR_t \tag{1)}$$

where E_t is the elevation of the wetland surface relative to mean sea level at a given time; E_{t+1} is the annualised increase in elevation from E_t; $MAR_{E(t)}$ is the annual rate of mineral deposition at elevation E_t; $OAR_{E(t)}$ is the annual rate of organic matter addition at elevation E_t; AC_t is the annual rate of autocompaction at elevation E_t; and SLR_t is the annual increment of SLR. As per previous simulations, empirical data from radiometrically dated sediment cores was used to calibrate mineral (MAR) and organic matter (OAR) addition rate functions (*Buffington et al.*, 2021; *Mudd et al.*, 2009; *Thorne et al.*, 2018). In our adapted model, the MAR, OAR and AC sub-models were functions of elevation and time, as per equations 2, 3 and 4, respectively. Model calibration was undertaken at the sub-site level as differences in mineral sediment supply and vegetation structure were evident between sub-sites (*Rogers and Saintilan*, 2021). This provided the opportunity to consider the influence of varying sediment supply and plant productivity on model simulations.

2.3 Sub-model set-up

Sediment cores were extracted from the mangrove and saltmarsh at each sub-site in 2017. Cores were located within the middle of the zone where SET-MHs were positioned, and the surface elevation at each core location was recorded using a real-time kinematic global positioning system. Cores were split longitudinally and subsampled at every cm in the top 10 cm of the soil profile, and every 5 cm afterwards to a core depth of 1 m. Grain size was determined for each sample using a Malvern Mastersizer 2000 laser diffractometer. Samples were oven dried to constant weight at 60°C and dry bulk density was estimated as the ratio of the dry sample mass to the wet sample volume. Samples were homogenised using a Retsch three-dimensional vibrator mill (Type-MM-2: Haan, Germany) and analysed for percentage carbon using dry combustion techniques by the Environmental Analysis Laboratory at Southern Cross University. Detailed sediment characterisation is provided in *Rogers and Saintilan* (2021). Carbon concentration was converted to organic matter concentration using equations specifically developed for mangroves and saltmarshes in the study region that relate the proportion of carbon to the proportion of mass lost on ignition (LOI) (*Owers et al.*, 2016). Grain size composition (%), dry bulk density (g cm^{-3}), proportion of organics and inorganics (%), organic and inorganic concentrations (g cm^{-3}), mineral concentrations (g cm^{-3}), and carbon concentrations (%) at various depths are provided in Figure S1.

To determine organic and inorganic matter addition rates, the total organic matter and the total inorganic matter was determined over substrate depths of known age. The age of accumulated material at various depths was determined using ^{210}Pb dating techniques applied to the same cores analysed for carbon concentration and reported in detail in *Rogers et al.* (2022). As per *Rogers et al.* (2022), the constant rate of supply model was used to determine sediment ages and results of ^{210}Pb analyses are provided in Figure S2.

$$OAR = \sum_{a}^{0} o\rho_s \qquad 2)$$

$$MAR = \sum_{a}^{0} (1-o)\rho_s \qquad 3)$$

where a is depth, based on approximately 50 years of sedimentation determined from ^{210}Pb profiles, ρ_s is bulk density, and o is organic matter concentration (%). The depth of a was based on the age of sediments at the base depth where organic material was concentrated within sediment profiles and ranged between 48 years at depth of ~ 35 cm in the mangrove at French Island to 148 years at a depth of ~ 1 m in the mangrove at Rhyll Inlet.

To account for the varying contribution of organic matter to substrates between vegetation types, we used a vegetation zonation approach that accounted for the influence of elevation or inundation on vegetation zonation. The vertical distribution of mangrove and saltmarsh zones was determined from mapping of vegetation boundaries from contemporary aerial photography, as detailed in *Rogers et al.* (2022), and extracting elevation statistics of boundaries at each sub-site via analyses with a LiDAR-derived digital elevation model (see Table S1 for values). For the mangrove zone, organic matter addition was presumed to be negligible for elevations at or below the median elevation of the seaward mangrove boundary and the upper 75% quantile of the landward mangrove boundary. For the saltmarsh zone, organic matter addition was presumed to be negligible at the lower 25% quantile of the seaward boundary and at the modelled elevation of the highest astronomical tide. The modelled highest astronomical tide elevation was used to delimit the landward extent of saltmarsh, rather than elevation statistics extracted from mapping of the landward saltmarsh boundary, as the landward extent is heavily influenced by adjoining land uses and drainage and is therefore not likely to be indicative of the true landward saltmarsh limit. As the landward mangrove boundary and the seaward saltmarsh boundary are mapped as the same feature, using the 75% quantile for the mangrove landward boundary and 25% quantile for the saltmarsh seaward boundary accommodated overlap between these zones. Vegetation transitions within later model simulations were parameterised to occur at the intersection between mangrove and saltmarsh OAR sub-models. The boundary elevations (m AHD) for mangrove and saltmarsh zones at each sub-site is provided in Table S1.

Sub-models described below were initially calibrated to the Australian height datum (AHD), where 0.000 m AHD represents mean sea level modelled from 30 tide gauges around the Australian coast between 1966 and 1968. Whilst 0.000 m AHD approximates mean sea level, there is reported to have been 1.4 ± 0.3 mm yr^{-1} sea-level rise around the Australian coast in the period 1966-2009 (*White et al.*, 2014). Accordingly, AHD is not a definitive indication of elevations with respect to mean sea level and does not account for increases to mean tidal level due to sea-level rise. In addition, applying the model with respect to absolute elevation does not accommodate variation in tidal range that can occur between sites. To accommodate these factors within simulations, we followed the approach of earlier sea level environmental reconstruction studies (*B Horton et al.*, 1999; *Kemp et al.*, 2013; *Lal et al.*, 2020) and WARMER experiments (*Buffington et al.*, 2021; *Thorne et al.*, 2018) by recalibrating all sub-models to the tidal frame at each sub-site using a unitless measure of relative elevation that accounts for variation in tidal range between sub-sites and facilitates comparisons between sub-sites. In this study, position within the tidal frame (z) was delimited by the model boundaries, whereby coastal wetland vegetation largely occurs between mean tide level and highest astronomical tide.

$$z = \frac{E - MTL}{HAT - MTL} \quad 4)$$

where E is the elevation with respect to AHD, and mean tide level (MTL) and highest astronomical tide (HAT) are defined with respect to AHD.

To determine mean tide level, processed data of mean minimum, mean and mean maximum monthly water level were accessed for the Stony Point tide gauge for the full record length. Linear regression analyses were applied to the mean water level to determine mean tide level (MTL) at the tide gauge at the time of core extraction (see Figure S3, Table S2). A similar approach was applied to the mean maximum monthly water level to determine the maximum tide level at the tide gauge at the time of core extraction. Rogers et al. (2022) calibrated site-specific water-level data derived from Hobo water-level loggers against tide gauge data to ascertain the degree of tidal modification that occurs within Westernport Bay. For this study, highest astronomical tide was identified as the maximum monthly water level at the time of core extraction, estimated on the basis of linear regression analyses, with an additional tidal modification factor. Water level data, tidal modification factors from Rogers et al. (2022), elevation of vegetation zonation boundaries and the position in the tidal frame of vegetation zonation boundaries are provided in Table S3.

2.4 Sub-model calibration

Mineral sediment accretion has been shown in previous studies (*Cahoon and Reed*, 1995; *Palinkas and Engelhardt*, 2019) and at this study site to be linearly related to elevation, accommodation space or inundation frequency (*Rogers and Saintilan*, 2021; *Rogers et al.*, 2022); and provided confidence that linear relationships would be suitable for the $MAR_{E(t)}$ sub-model. Linear relationships were established between MAR and elevation using data from mangrove and saltmarsh cores at each sub-site. We presumed negligible mineral sediment accretion at the landward boundary where accommodation space is limited, modelled as the limit of HAT. WARMER-2 (*Buffington et al.*, 2021) proposed high MAR at lower elevations was unrealistic, and presumed that erosion did not occur; they accounted for this by developing a model that balances sediment deposition flux. This modification was not incorporated in this study as it was anticipated that the autocompaction sub-model would adjust for this process. Validation of the autocompaction model at the study site by *Rogers et al.* (2022) confirm that this is a reasonable assumption. MAR sub-model parameterisation and calibration, with respect to z, are provided in Figure S4 andd Table S4. *Rogers et al.* (2022) report on tidal impoundment within abandoned salt evaporative ponds in the saltmarsh at French Island and indicate that this has important implications for both mineral and organic matter addition at this location. The French Island MAR models was subsequently recalibrated to indicate a linear relationship between mineral accretion in the mangrove zone and no mineral accretion at the limit of tidal inundation.

Organic matter addition has been related to elevation using a second-order polynomial, as per *James T. Morris et al.* (2002) and parameterised in the *Marsh Equilibrium Model* (*James T Morris et al.*, 2021), and peak models may describe the relationship between $OAR_{E(t)}$ and elevation better than linear models at the study site (*Rogers and Saintilan*, 2021). Second-order polynomial relationships were established between OAR and elevation using data from mangrove and saltmarsh cores and presuming negligible OAR at the boundaries of each vegetation zone. OAR sub-model parameterisation and calibration, with respect to z, are provided in Figure S5 and Table S5. The position within the tidal frame (z) (tidal position) at which transitions between vegetation zones would be simulated was parameterised to occur at the intersection between mangrove and saltmarsh OAR sub-models. To validate this assumption, we established the tidal position (z) at the mapped mangrove-saltmarsh boundary in 2009 and compared this value to the tidal position of the intersection between mangrove and saltmarsh OAR sub-models. Comparisons of the modelled and observed elevation of the landward mangrove boundary were undertaken and analysis of variance was applied to ascertain whether there was a significant difference in the modelled and observed elevations at each sub- site. Validation results and comparisons, provided in Table S6 and Figure S6, confirmed no significant difference between modelled and observed elevation at sub-sites ($p = 1.000$), and provided confidence in parameterisation of the tidal position of the mangrove-saltmarsh boundary.

To account for post-depositional processes of autocompaction, the relationship established between autocompaction and vertical accretion at the study site was adapted. This relationship was derived from a 20-year SET-MH monitoring record of vertical accretion and surface elevation gain that demonstrated that autocompaction was linearly related to vertical accretion, with approximately 80% of deposited sediment annually undergoing post-depositional autocompaction (*Rogers and Saintilan*, 2021). The established relationship was modified to ensure autocompaction was negligible at the elevation of the landward boundary, modelled as the limit of HAT. This modulation was directly applied to $MAR_{E(t)}$ to determine AC_t, and, whilst not directly related to elevation, it is implicitly related to elevation. AC_t sub-model parameterisation are provided in Figure S7 and Table S7.

2.5 Short-term model validation

For short-term validation, the model was set-up to run at the starting elevation of the SET located nearest to the point of core extraction and ran for a 20-year period corresponding to the period of SET measurements from October 2000. Sea-level rise was imposed on the model and estimated as approximately 3.03 mm yr-1 based on the rate of sea-level rise recorded at the nearest tide gauge between 2000 and 2017, a rate that is relatively consistent with global trends. Simulated surface elevations were then compared to the time-series of surface elevation change recorded at the nearest SET. To validate model performance, matched pairs t-test was undertaken to ascertain whether statistical differences existed between elevation measured using SETs and simulated elevations at each sub-site and within each zone. While SET measurements have a reported confidence of ± 1.5 mm (*Cahoon et al.*, 2002), considerable variability can arise due to the influence of the El Niño Southern Oscillation on substrate volumes at Westernport Bay (*K. Rogers et al.*, 2005). To account for this variability, comparisons were also made between the mean difference in SET measurements and simulations, and the mean standard error arising from SET measurements.

2.6 Medium-term model validation

For medium-term validation we followed the approach of *Mogensen and Rogers* (2018) by hindcasting elevations to an initial start date, running the model over the historical period using observed rates of sea-level rise, and then comparing the simulated elevations to contemporary elevations. For validation, we focussed on elevations near MTL as this is where the highest degree of change in elevation is likely to occur, and at the landward mangrove boundary. The utility in validating the landward saltmarsh boundary is limited because this boundary is high in the tidal frame and less influenced by bio-morphodynamic changes (Rogers et al. in review) due to low rates of tidal inundation and sediment addition. In addition, this boundary is generally more influenced by human interventions, such as drainage, infilling and disturbance.

Prior to validation simulations, validation set-up was required to identify starting elevations for simulations and expected elevations for comparison with simulation outputs. Linear regression analyses of mean monthly tide gauge data (Figure S3 and Table S2) indicated that mean tide level was approximately 0.03 m in 2009, which was at or near the seaward limit of mangroves based on digitisation of mangrove boundaries on high resolution imagery from 2009 (Table S1). Following confirmation that the mangrove seaward boundary approximated mean tide level, the seaward and landward boundaries of the mangrove at each sub-site was digitised from aerial photography near the commencement of tide gauge records at Stony Point. Aerial photography from 1973/74 was collected in colour and at high resolution, thereby providing improved capacity to map the mangrove seaward boundary. The mapping of these boundaries has been presented in Rogers et al. (2022). Using linear regression analyses provided in Figure S3 and parameters in Table S2, mean tide level and highest astronomical tide was hindcast to the time of digitised historic aerial photography (i.e. 1973/74). The mapped seaward boundary in 1974 was presumed to have an elevation at or near the elevation of the hindcast mean tide level. To hindcast the elevation of the mapped landward mangrove boundary in 1974, we first defined the approximate position in the tidal frame of this boundary in 2009 using Equation 1. Using hindcast values of mean tide level and highest astronomical tide we then resolved the starting elevation for simulations of the landward mangrove boundary in 1974. Hindcast elevation of the seaward and landward mangrove boundaries in 1974 was used as the starting point for model simulations, and the model was projected to run from 1974 until 2009 at each elevation. The modelled elevation at 2009 was compared to the expected elevation, which was defined as the elevation of the 1974 boundaries on the 2009 LiDAR-derived DEM. Matched pairs t-test was applied to test whether significant differences between the expected and modelled elevations were evident.

2.7 Long-term model validation

For long-term validation, the model was run for a period of 2020 years over the Holocene. There remains ongoing debate about the sea-level history over the mid to late Holocene for the Australian margin (*Lewis et al.*, 2013), with some authors proposing a highstand of approximately +1.5 m higher than present, and others finding no evidence of a highstand. This uncertainty remains for the study region, with only one fixed biological indicator, positioned within the zone of contemporary wave impact at an elevation of +1.5 m AHD, and other evidence of a highstand in the region is reportedly absent (*Kennedy et al.*, 2020). For the purposes of long-term model validation, we have presumed that sea level was stable for millennia, not only because there is insufficient evidence of a highstand, but also because model parameterisation was undertaken based on conditions of low rates of sea-level rise, not sea-level fall as would have occurred following a mid-late Holocene high stand.

Whilst it is likely that the tidal regime across Westernport Bay has changed over the late Holocene, we have limited data for parameterisation and therefore presumed the tidal range was consistent with contemporary conditions for the period of model validation simulations. All other variables were also based on contemporary model parameterisation. The model was parameterised for each sub-site for a period of 2020 years, with 1900 years based on stable sea-level conditions, and the remaining 120 years based on observations of 20th and 21st century sea-level rise acceleration reported by the Intergovernmental Panel on Climate Change (IPCC) (*Fox-Kemper et al.*, 2021). The outcome was that mean sea level was hindcast to 1900, and this was used as the starting elevation for model simulations. The IPCC specifically report SLR of 0.20 (0.15-0.25) m rise over the period 1901-2018, with considerable acceleration from a median rate of 1.35 (0.78-1.92) mm yr^{-1} between 1901 and 1990, 2.33 (1.55-3.12) mm yr^{-1} between 1971 and 2018, 3.25 (2.88-3.61) mm yr^{-1} between 1993 and 2018, and 3.69 (3.21-4.17) mm yr^{-1} between 2006 and 2018. For long-term validation we parameterised the 20th and 21st century sea-level rise scenarios as accelerating from 1.35 mm yr^{-1} between 1901-1970, to 1.73 mm yr^{-1} between 1971-1993, and 3.69 mm yr^{-1} between 2006-2020. We confirmed that model simulations equilibrated at the top of the tidal frame before the commencement of the 20th century, and this elevation was presumed to represent equilibrium elevation prior to the 20th century sea-level rise acceleration. We then determined the elevation of what was the equilibrium elevation prior to the 20th and 21st century sea-level rise.

We compared these simulated values to 'real' elevations at Westernport Bay by presuming that the saltmarsh at each sub-site represents the former equilibrium elevation. Transects were extracted from a LiDAR-derived digital elevation model that indicates elevation at 2009. These transects confirmed that the mapped *Tecticornia* and herbaceous saltmarsh zones exhibited negligible slope. The average elevation of the saltmarsh plain along each transect was then determined for comparison with the simulated elevation at 2009.

3 Results

3.1 Short-term validation

SET measurements corresponded reasonably well with model simulations over the period 2000-2020 (Figure 2), particularly given the reported variation in SET measurements at Westernport Bay (*K. Rogers et al.*, 2005). Matched pairs t-tests indicated high correlation between the SET measurements and model simulations at each study location (Table 1). At French Island, the model simulated lower rates of surface elevation gain in the saltmarsh than was observed from SET measurements ($p = 0.0008$); this was not surprising given the tidal impoundment that occurs at this location following abandonment of evaporative salt ponds (*Rogers and Saintilan*, 2021). At Kooweerup, the model tended to simulate higher rates of surface elevation gain in the saltmarsh ($p = 0.0007$). Significant differences in SET measurements and model simulations were also evident at Quail Island in the mangrove ($p = 0.0468$) and saltmarsh ($p = 0.0247$); however, this sub-site exhibits considerable variability in SET measurements and the mean difference in SET measurement and simulations did not exceed the mean standard error arising from SET measurements. Excluding the saltmarsh at French Island, the mean difference between model simulations and SET observations was ≤ 0.02 m, and this provided considerable confidence in model performance over the 20-year time frame.

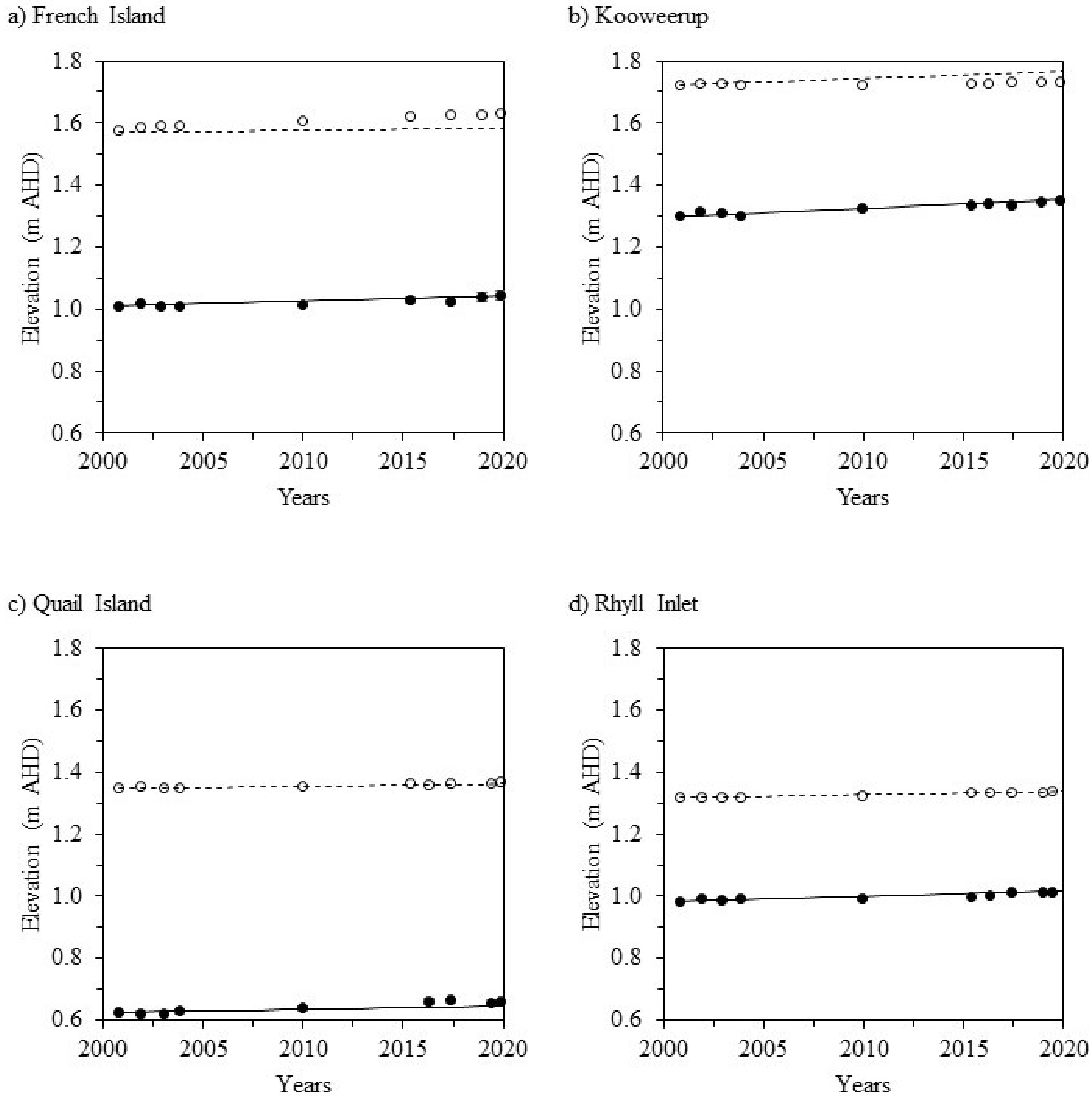

Figure 2. Comparisons for SET observations and model simulations in the mangrove and saltmarsh at a) French Island, b) Kooweerup, c) Quail Island, and d) Rhyll Inlet. Mangrove and saltmarsh SET measurements indicated by closed circles and open circles respectively; mangrove and saltmarsh simulations indicated by solid and dashed lines, respectively.

Table 1. Matched pairs t-test statistics comparing model simulations (m AHD) to SET measurements (M AHD)at each subsite. * denotes significant differences at significance level of 0.05; † denotes zones within sub-sites where the mean difference in SET measurements and simulations exceeded the mean standard error of SET measurements.

Sub-Site	**French Island**		**Kooweerup**		**Quail Island**		**Rhyll Inlet**	
Zone	Mangrove	Saltmarsh	Mangrove	Saltmarsh	Mangrove	Saltmarsh	Mangrove	Saltmarsh
Mean Difference	0.0027	-0.033	0.0009	0.02	-0.008	-0.002	0.0023	0.0004
Standard Error	0.002	0.0066	0.002	0.0042	0.0035	0.0008	0.0015	0.0006
Correlation	0.917	0.9925	0.9665	0.8828	0.9739	0.9676	0.9341	0.9712
t-Ratio	1.345	-4.985	0.4674	4.8152	-2.303	-2.64	1.5251	0.615
Prob > |t|	0.2115	0.0008*	0.6502	0.0007*	0.0468*	0.0247*	0.1555	0.5511
Prob > t	0.1058	0.9996	0.3251	0.0004*	0.9766	0.9876	0.0777	0.2755
Prob < t	0.8942	0.0004*	0.6749	0.9996	0.0234*	0.0124*	0.9223	0.7245
SET Mean Standard Error	0.0096	0.0033†	0.0044	0.0035†	0.0111	0.013	0.0026	0.0027

3.2 Medium-term validation

Model simulations between 1974 and 2009 (Figure 3) and comparison with elevations at 2009 extracted from a LiDAR-derived DEM confirmed reasonable agreement (Table 2) between modelled elevations and expected elevations. Matched pairs t-test confirmed no statistical difference between expected and modelled elevations for both the seaward and landward mangrove boundary (Prob > |t| = 0.2605, Prob > t = 0.1302, Prob < t = 0.8698).

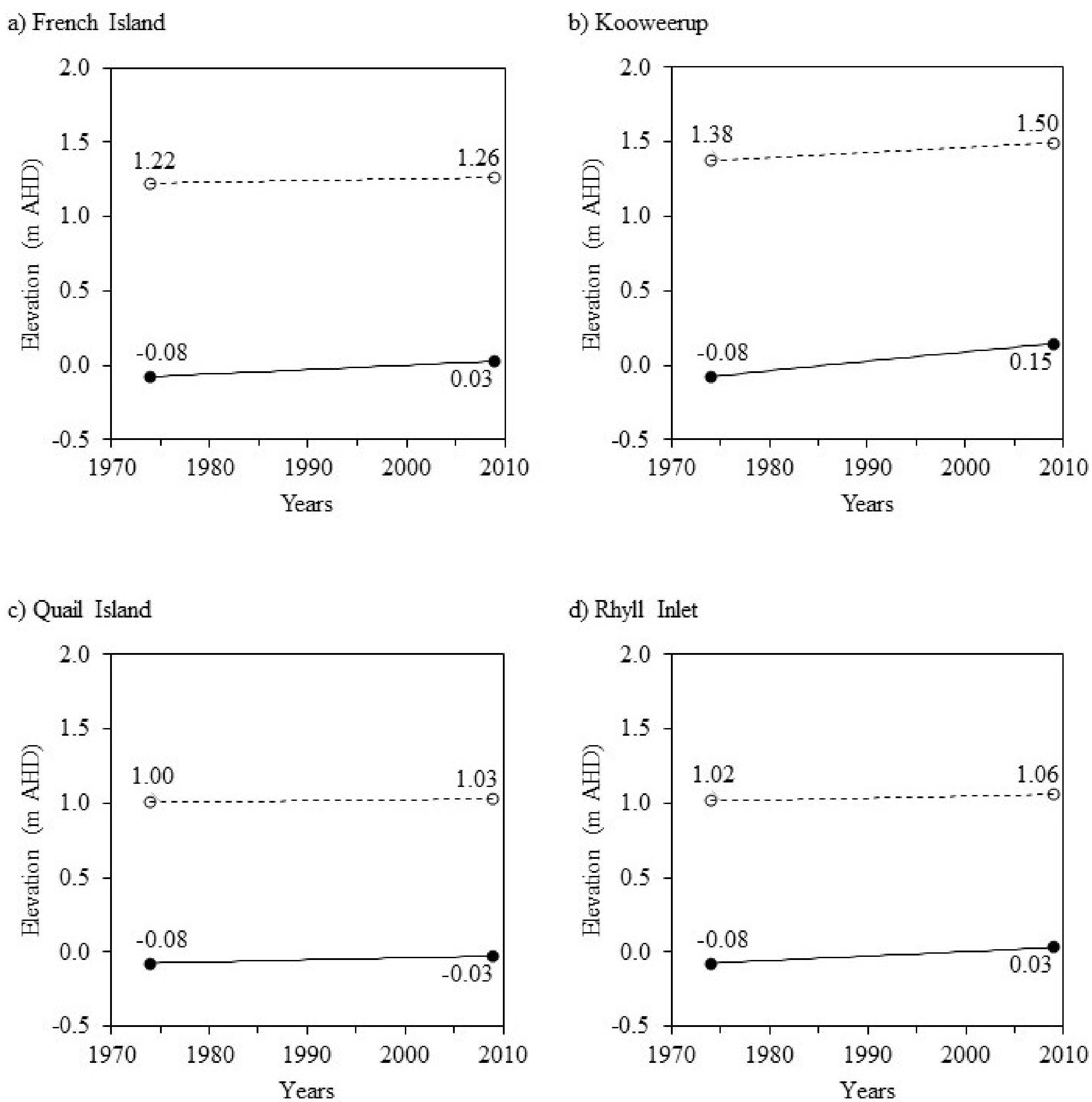

Figure 3. Simulated elevation change between 1974 and 2009 for the seaward and landward mangrove boundaries at a) French Island, b) Kooweerup, c) Quail Island, and d) Rhyll Inlet. Mangrove and saltmarsh simulations indicated by solid lines and dashed lines, respectively.

Table 2. Estimated tidal position of the seaward and landward mangrove boundary at each sub-site, hindcast elevation (m) of each boundary at 1974, modelled elevation of each boundary at 2009, expected elevation of each boundary at 2009 based on extraction from a LiDAR-derived digital elevation model, and difference between expected and modelled elevation. [1]Start elevation for model simulations.

Sub-site	Mangrove Boundary	Position in Tidal Frame(z)	Hindcast Elevation (m AHD)[1]	Modelled Elevation (m AHD)	Expected Elevation (m AHD)	Difference (m)
French Island	Seaward	0.00	-0.08	0.03	0.00	-0.03
	Landward	0.77	1.22	1.26	1.33	0.07
Kooweerup	Seaward	0.00	-0.08	0.15	0.25	0.10
	Landward	0.66	1.38	1.50	1.48	-0.02
Quail Island	Seaward	0.00	-0.08	-0.03	-0.13	-0.10
	Landward	0.60	1.00	1.03	1.11	0.08
Rhyll Inlet	Seaward	0.00	-0.08	0.03	0.12	0.09
	Landward	0.69	1.02	1.06	1.12	0.06

3.3 Long-term validation

Profiles at each study location confirmed that substrate elevations within the saltmarsh were relatively stable with slopes of < 0.01 (Figure 4). Comparison of modelled elevations at 2009 against LiDAR-derived mean elevations of the saltmarsh indicated that modelled simulations were within 0.06 m of expected elevations for each sub-site, except Quail Island (Table 3), and lie well within the range of the reported vertical accuracy of the LiDAR data set. Given the position of the Quail Island sub-site along a tidal creek where accommodation space is limited, it is not surprising that the discrepancy between the expected and modelled elevation at this site was substantial. Matched pairs t-tests for all sites confirmed reasonable agreement (Prob $> |t| = 0.1335$, Prob $> t = 0.0668$, Prob $< t = 0.9322$), but imply a tendency to marginally underestimate elevations.

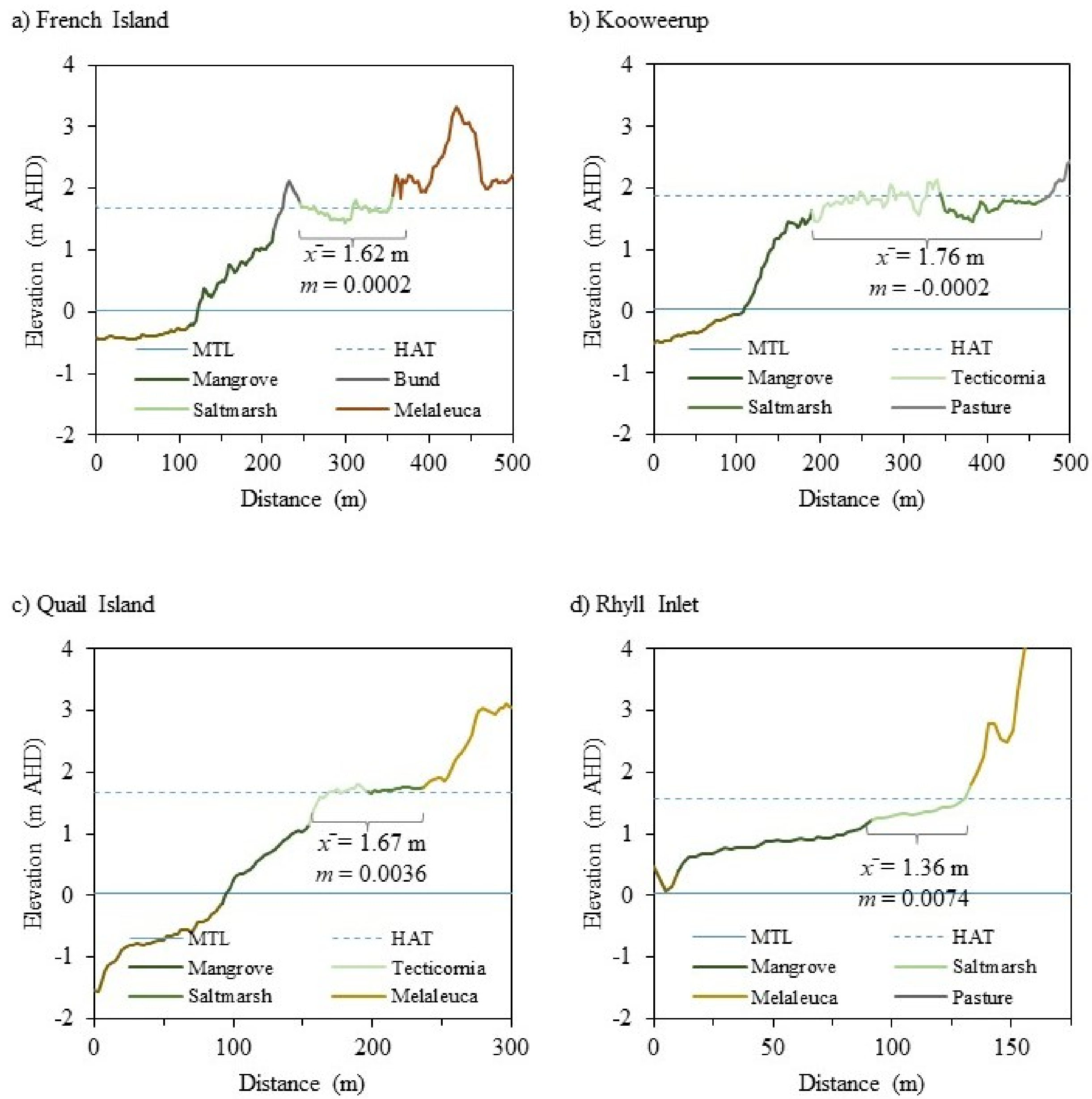

Figure 4. Substrate profile, and mean elevation and slope of the saltmarsh at a) French Island, b) Kooweerup, c) Quail Island and d) Rhyll Inlet.

Table 3. Modelled equilibrium elevations at 1900, modelled elevations of the former equilibrium elevation at 2009 and expected elevation at 2009, as per Figure 4 and based on extraction from a LiDAR-derived DEM.

Sub-site	Equilibrium elevation at 1900 (m AHD)	Modelled elevation (m AHD)	Expected elevation (m AHD)	Difference (m)
French Island	1.53	1.57	1.62	-0.05
Kooweerup	1.68	1.77	1.76	+0.01
Quail Island	1.39	1.44	1.67	-0.23
Rhyll	1.38	1.42	1.36	+0.06

4 Discussion

4.1 Model Performance

Model validation is rarely undertaken for coastal wetland evolution models, and this largely arises from the difficulty in hindcasting models and generating a substrate surface for comparison of hindcasts (*Wiberg et al.*, 2020). Accordingly, models are typically forecast from a previous elevation and then compared to contemporary conditions (*Mogensen and Rogers*, 2018). In the few locations where repeat elevation surveys are available, either from LiDAR data or measurements of surface elevation change, models could be validated; however, this short validation period limits the capacity to apply models with confidence beyond the validation period. In this study, considerable effort was placed on calibrating sub-models using real data from across a range of sub-sites that exhibit varying rates of mineral and organic matter addition, and then validating the model across a range of timescales extending from the observational period (~20 years) to a few millennia.

High correlation between model simulations and SET measurements was established during short-term validation against observational records. Some statistically significant differences were detected between SET measurements, particularly in the saltmarsh zones where tidal modification influences rates of organic matter accumulation. For example, tidal impoundment associated with abandoned salt ponds has favoured organic matter accumulation, resulting in observed rates of surface elevation gain exceeding model simulations (*Rogers and Saintilan*, 2021). The inverse pattern was evident at Kooweerup and may arise due to ditching at the back of the saltmarsh modifying drainage and favouring organic matter decomposition. While-t tests indicated some statistically significant differences, the record of observations may not sufficiently describe the variation in SET measurements over time. Assessment of differences between observations and simulations in the context of the error in SET measurements indicates that it is only in the saltmarsh at French Island and Kooweerup where differences exceed the error. Modifying tidal behaviour is reported to influence restoration success (*Glamore et al.*, 2021), and on-going monitoring of the influence of tidal modification of surface elevation trajectories is recommended.

Comparison with changes observed in the seaward and landward boundary of the mangroves in aerial photography between 1974 and 2009 indicated reasonable agreement over the 35-year model projection period. The greatest discrepancy, in the order of +0.10 m, was evident at the seaward boundary at Kooweerup, where rapid shoreline progradation has been documented. A similar discrepancy of -0.10 m is evident at the seaward boundary at Quail

Island; a shoreline on the margins of a channel that is highly dynamic (*Rogers and Saintilan*, 2021). Large trees and associated canopy overhang likely limit the capacity to effectively map the shoreline position at this location, and it is reasonable to assume that some of this discrepancy is related to mapping errors of commission (*Rogers et al.*, 2022). Based on model assumptions regarding rates of sea-level rise over this 35-year projection period, this discrepancy is regarded to be acceptable; this is further supported by statistical analyses indicating no significant difference between the expected and modelled elevations.

Based on millennia of substrate evolution under relatively stable sea levels, model discrepancy was greatest in the saltmarsh at Quail Island, the location with the lowest rate of substrate elevation gain and the steepest saltmarsh slope, implying that equilibrium may not have been achieved over this timescale. At sites where the saltmarsh slope was very low, rates of sediment supply are high and where it is reasonable to presume that equilibrium was achieved within the saltmarsh, discrepancies ranged between +0.06 m and -0.05 m; a remarkably small value given the duration of model projection.

4.2 Model application

Following validation, we have some confidence that the 0D model could be used to explore a range of future and/or hypothetical scenarios of coastal wetland evolution. However, 0D models, by design, only describe vertical adjustment of a point through time and whilst they are the basis for spatial modelling and mapping, their application in three dimensions requires further consideration. Currently, the model has been calibrated using spatially explicit, single-point data, including data from eight cores that were analysed for organic matter content and to develop a chronology of sediment supply, and 24 SET-MH that were used to develop the autocompaction sub-model. As the autocompaction model is largely based on sediment accretion, rates of sediment supply and mineral and organic matter addition will require consideration of spatial variation across Westernport Bay. Hydrodynamic modelling is typically advocated as the best approach for modifying sediment supply yet remains computationally intensive to apply dynamically. Additionally, there are few examples where hydrodynamic modelling has been dynamically applied to project the response of coastal wetlands to sea-level rise (*Kumbier et al.*, 2022). Given the scale of Westernport Bay, this is not currently a feasible option, and geomorphological approaches that consider spatial controls on sediment supply remain the best approach. This could include coastal system mapping (*J French et al.*, 2016a; *J R French et al.*, 2016b) to identify shoreline units that behave with some consistency, segmenting the bay on the basis of variation in tidal range (*Mogensen and Rogers*, 2018; *Rogers et al.*, 2019b) or modifying the coastal compartment approach to apply to a large marine embayment (*Davies*, 1974; *Thom et al.*, 2018).

As 0D models focus on vertical adjustment, they are limited in their ability to simulate lateral changes as they presume no transport of sediment following deposition. Therefore 0D models that focus on vertical adjustment are not able to simulate shoreline erosion or lateral creek extension, and coupling of the vertical 0D model with lateral models that simulate shoreline erosion and creek extension may be required. Shoreline erosion is evident on the northeastern shoreline of Westernport Bay where fetch is greatest and active cliff erosion is occurring (*Water Technology*, 2014), but is not currently evident along any of the shorelines supporting coastal wetlands. Where fetch operates parallel to shorelines on the Northern Arm there remains considerable lateral space, expansive tidal flats and high sediment supply within

Westernport Bay (*Hancock et al.*, 2001; *Rogers et al.*, 2022); and it is reasonable to presume that shorelines of the Northern Arm may not be exposed to considerable erosion. Furthermore, it has been proposed that where shoreline extent is low relative to coastal wetland extent, models operating in the vertical dimension may be sufficient (*Wiberg et al.*, 2020), and have been applied in three dimensions (*Schile et al.*, 2014; *Thorne et al.*, 2018). However, there is increasing evidence from the USA that shoreline erosion is linked to vertical accretion, with sediments eroded from shorelines being redistributed to inner marsh environments (*Hopkinson et al.*, 2018), a process somewhat similar to the proposed roll-back of estuarine shorelines (*Elliott et al.*, 2014). This process has been incorporated into models (*Kirwan and Murray*, 2008), and could be considered for coastal wetlands on the margins of channels, such as Quail Island. Additionally, there is evidence of expanding creek networks (*Whitt et al.*, 2020) that have facilitated lateral expansion of mangroves into saltmarshes throughout Westernport Bay and tidal creek extension has been related to sea-level rise. The model should be tested in three dimensions to determine its capacity to simulate tidal creek extension or coupled with a creek extension model to effectively capture this process.

5 Conclusions

Model calibration improved upon previous attempts which simplified autocompaction; this was achieved by incorporating an autocompaction model derived from a 20-year record of measurements of surface elevation gain and vertical accretion. Overall, the model framework performed well at the medium to long-term scale and was within the range of variability reported in measurements of surface elevation change from the network of SET-MH at Westernport Bay at the short-term scale. Validation across a range of temporal scales and sub-sites has provided the confidence needed to apply this model to consider coastal wetland evolution under future sea-level rise scenarios. Model performance is founded upon robust, site-specific data collected relative to a range of timescales and model calibration for local conditions, in this case recognising the varying contribution of mangrove and saltmarsh vegetation to substrate elevations. We emphasise the critical need for site-specific data collection to calibrate and validate models. This step is too often ignored because of the resources required to collect data and the ease in extrapolating data from elsewhere to simulate marsh evolution. We now have the necessary confidence in the model framework to consider projections based on future scenarios of sediment accumulation and sea-level rise. Further work is required to apply the model in three dimensions to generate a landscape scale model, with specific consideration given to lateral changes in wetland extent.

Acknowledgments

We acknowledge the custodians of the Western Port area, the Bunurong (Boonerwrung) people of the Kulin Nation. We recognise the contribution of field and laboratory assistances in undertaking this work; over >20 years of analysis there are many to mention, but we remember each field trip and discussion fondly. Special thanks to Lawrance Ferns who has supported this research and the Victorian Government who has provided financial support with the initial establishment and recent measurements. This research is also partly supported by the Australia Research Council DP2100100739. The authors are not aware of any conflicts of interest.

Open Research

Datasets associated with this paper (DOI: 10.5281/zenodo.7672762) are archived at https://zenodo.org/record/7672762#.ZAgXCHZBybg. Codes associated with the model and simulations (DOI: 10.5281/zenodo.7707368) are archived at https://github.com/oxanarepina/IWEM0D.

References

Adam, P. (2009), Australian saltmarshes in global context, in *Australian saltmarsh ecology*, edited by N. Saintilan, pp. 1-22, CSIRO Publishing, Collingwood, Victoria, Australia.

Allen, J. R. L. (2000), Morphodynamics of Holocene salt marshes: a review sketch from the Atlantic and Southern North Sea coasts of Europe, *Quaternary Science Reviews*, *19*(12), 1155-1231.

Barbier, E. B., S. D. Hacker, C. Kennedy, E. W. Koch, A. C. Stier, and B. R. Silliman (2011), The value of estuarine and coastal ecosystem services, *Ecological Monographs*, *81*(2), 169-193, doi:10.1890/10-1510.1.

Boon, P. I., et al. (2015), Coastal wetlands of Victoria, south-eastern Australia: providing the inventory and condition information needed for their effective management and conservation, *Aquatic Conservation: Marine and Freshwater Ecosystems*, *25*(4), 454-479, doi:10.1002/aqc.2442.

Breithaupt, J. L., J. M. Smoak, R. H. Byrne, M. N. Waters, R. P. Moyer, and C. J. Sanders (2018), Avoiding timescale bias in assessments of coastal wetland vertical change, *Limnology and Oceanography*, *63*(S1), S477-S495.

Bridgewater, P. B., and I. D. Cresswell (1999), Biogeography of mangrove and saltmarsh vegetation: implications for conservation and management in Australia, *Mangroves and Salt Marshes*, *3*(2), 117-125.

Buffington, K. J., C. N. Janousek, B. D. Dugger, J. C. Callaway, L. M. Schile-Beers, E. Borgnis Sloane, and K. M. Thorne (2021), Incorporation of uncertainty to improve projections of tidal wetland elevation and carbon accumulation with sea-level rise, *PLoS ONE*, *16*(10), e0256707.

Cahoon, D. R., J. C. Lynch, P. Hensel, R. Boumans, B. C. Perez, B. Segura, and J. W. Day, Jr. (2002), High-precision measurements of wetland sediment elevation: I. Recent improvements to the Sedimentation-Erosion Table, *Journal of Sedimentary Research*, *72*(5), 730-733, doi:10.1306/020702720730.

Cahoon, D. R., and D. J. Reed (1995), Relationships among Marsh Surface Topography, Hydroperiod, and Soil Accretion in a Deteriorating Louisiana Salt Marsh, *Journal of Coastal Research*, *11*(2), 357-369.

Clark, J. A., and C. S. Lingle (1979), Predicted relative sea-level changes (18,000 years B.P. to present) caused by late-glacial retreat of the Antarctic Ice Sheet, *Quaternary Research*, *11*(3), 279-298, doi:http://dx.doi.org/10.1016/0033-5894(79)90076-0.

Davies, J. L. (1974), The coastal sediment compartment, *Australian Geographical Studies*, *12*(2), 139-151, doi:10.1111/j.1467-8470.1974.tb00270.x.

Doody, J. P. (2004), 'Coastal squeeze'— an historical perspective, *Journal of Coastal Conservation*, *10*(1), 129-138, doi:10.1652/1400-0350(2004)010[0129:csahp]2.0.co;2.

Dougherty, A. J., Z. A. Thomas, C. Fogwill, A. Hogg, J. Palmer, E. Rainsley, A. N. Williams, S. Ulm, K. Rogers, and B. G. Jones (2019), Redating the earliest evidence of the mid-Holocene relative sea-level highstand in Australia and implications for global sea-level rise, *Plos one*, *14*(7), e0218430.

Elliott, M., N. D. Cutts, and A. Trono (2014), A typology of marine and estuarine hazards and risks as vectors of change: a review for vulnerable coasts and their management, *Ocean and Coastal Management*, *93*, 88-99.

Fagherazzi, S., et al. (2012), Numerical models of salt marsh evolution: Ecological, geomorphic, and climatic factors, *Reviews of Geophysics*, *50*(1), RG1002, doi:10.1029/2011rg000359.

Fagherazzi, S., G. Mariotti, N. Leonardi, A. Canestrelli, W. Nardin, and W. S. Kearney (2020), Salt marsh dynamics in a period of accelerated sea level rise, *Journal of Geophysical Research: Earth Surface*, *125*(8), e2019JF005200, doi:10.1029/2019JF005200.

Fox-Kemper, B., et al. (2021), Ocean, Cryosphere and Sea Level Change, in *Climate Change 2021: The Physical Science Basis. Contribution of Working Group I to the Sixth Assessment Report of the Intergovernmental Panel on Climate Change*, edited by V. Masson-Delmotte, et al., Cambridge University Press.

French, J., H. Burningham, G. Thornhill, R. Whitehouse, and R. J. Nicholls (2016a), Conceptualising and mapping coupled estuary, coast and inner shelf sediment systems, *Geomorphology*, *256*, 17-35.

French, J. R., H. Burningham, G. D. Thornhill, and R. J. Nicholls (2016b), Integrating estuarine, coastal and inner shelf sediment systems in a common conceptual framework as a basis for participatory shoreline management, in *Geomorphology and Society*, edited, pp. 245-277, Springer.

Glamore, W., D. Rayner, J. Ruprecht, M. Sadat-Noori, and D. Khojasteh (2021), Eco-hydrology as a driver for tidal restoration: Observations from a Ramsar wetland in eastern Australia, *PLoS ONE*, *16*(8), e0254701.

Hancock, G. J., J. M. Olley, and P. Wallbrink (2001), Sediment transport and accumulation in Western Port: Report on Phase I of a study determining the sources of sediment to Western Port*Rep.*, 54 pp, CSIRO, Canberra.

Hopkinson, C. S., J. T. Morris, S. Fagherazzi, W. M. Wollheim, and P. A. Raymond (2018), Lateral marsh edge erosion as a source of sediments for vertical marsh accretion, *Journal of Geophysical Research: Biogeosciences*, *123*(8), 2444-2465.

Horton, B., R. Edwards, and J. Lloyd (1999), A foraminiferal-based transfer function: implications for sea-level studies, *The Journal of Foraminiferal Research*, *29*(2), 117-129.

Horton, B. P., I. Shennan, S. L. Bradley, N. Cahill, M. Kirwan, R. E. Kopp, and T. A. Shaw (2018), Predicting marsh vulnerability to sea-level rise using Holocene relative sea-level data, *Nature Communications*, *9*(1), 1-7.

Hughes, A., I. Prosser, P. Wallbrink, and J. Stevenson (2003), Suspended sediment and bedload budgets for the Western Port Bay Basin*Rep.*, CSIRO, Canberra.

Kemp, A. C., R. J. Telford, B. P. Horton, S. C. Anisfeld, and C. K. Sommerfield (2013), Reconstructing Holocene sea level using salt-marsh foraminifera and transfer functions: lessons from New Jersey, USA, *Journal of Quaternary Science*, *28*(6), 617-629.

Kennedy, D. M., T. S. Oliver, T. Tamura, C. V. Murray-Wallace, B. G. Thom, N. J. Rosengren, D. Ierodiaconou, P. Augustinus, C. Leach, and J. Gao (2020), Holocene evolution of the Ninety Mile Beach sand barrier, Victoria, Australia: The role of sea level, sediment supply and climate, *Marine Geology*, *430*, 106366.

Khan, N. S., E. Ashe, T. A. Shaw, M. Vacchi, J. Walker, W. Peltier, R. E. Kopp, and B. P. Horton (2015), Holocene relative sea-level changes from near-, intermediate-, and far-field locations, *Current Climate Change Reports*, *1*(4), 247-262.

Khojasteh, D., S. Chen, S. Felder, V. Heimhuber, and W. Glamore (2021), Estuarine tidal range dynamics under rising sea levels, *PLoS ONE*, *16*(9), e0257538.

Kirwan, M. L., and A. B. Murray (2008), Ecological and morphological response of brackish tidal marshland to the next century of sea level rise: Westham Island, British Columbia, *Global and Planetary Change*, *60*(3-4), 471-486.

Kumbier, K., K. Rogers, M. G. Hughes, K. K. Lal, L. A. Mogensen, and C. D. Woodroffe (2022), An Eco-Morphodynamic Modelling Approach to Estuarine Hydrodynamics & Wetlands in Response to Sea-Level Rise, *Frontiers in Marine Science*, *9*, 860910, doi:10.3389/fmars.2022.860910.

Lal, K. K., C. Bonetti, C. D. Woodroffe, and K. Rogers (2020), Contemporary distribution of benthic foraminiferal assemblages in coastal wetlands of south-eastern Australia, *Estuarine , Coastal and Shelf Science*, *245*, 106949.

Lewis, S. E., C. R. Sloss, C. V. Murray-Wallace, C. D. Woodroffe, and S. G. Smithers (2013), Post-glacial sea-level changes around the Australian margin: a review, *Quaternary Science Reviews*, *74*, 115-138, doi:http://dx.doi.org/10.1016/j.quascirev.2012.09.006.

Marani, M., C. Da Lio, and A. D'Alpaos (2013), Vegetation engineers marsh morphology through multiple competing stable states, *Proceedings of the National Academy of Sciences*, *110*(9), 3259-3263.

Mogensen, L. A., and K. Rogers (2018), Validation and Comparison of a Model of the Effect of Sea-Level Rise on Coastal Wetlands, *Scientific Reports*, *8*(1), 1369.

Morris, J. T., D. Cahoon, J. C. Callaway, C. Craft, S. C. Neubauer, and N. B. Weston (2021), Marsh equilibrium theory: Implications for responses to rising sea level, in *Salt marshes: Function, dynamics, and stresses*, edited by D. FitzGerald and Z. Hughes, Cambridge, doi:10.1017/9781316888933.009.

Morris, J. T., P. V. Sundareshwar, C. T. Nietch, B. Kjerfve, and D. R. Cahoon (2002), Responses of coastal wetlands to rising sea-levels, *Ecology*, *83*(10), 2869-2877, doi:doi:10.1890/0012-9658(2002)083[2869:ROCWTR]2.0.CO;2.

Mudd, S. M., S. M. Howell, and J. T. Morris (2009), Impact of dynamic feedbacks between sedimentation, sea-level rise, and biomass production on near-surface marsh stratigraphy and carbon accumulation, *Estuarine, Coastal and Shelf Science*, *82*(3), 377-389, doi:http://dx.doi.org/10.1016/j.ecss.2009.01.028.

Nicholls, R. J. (2011), Planning for the impacts of sea level rise, *Oceanography*, *24*(2), 144-157, doi:http://dx.doi.org/10.5670/oceanog.2011.34.

Oliver, T., K. Rogers, C. Chafer, and C. Woodroffe (2012), Measuring, mapping and modelling: an integrated approach to the management of mangrove and saltmarsh in the Minnamurra River estuary, southeast Australia, *Wetlands Ecology and Management*, *20*(4), 353-371, doi:10.1007/s11273-012-9258-2.

Owers, C. J., K. Rogers, D. Mazumder, and C. D. Woodroffe (2016), Spatial Variation in Carbon Storage: A Case Study for Currambene Creek, NSW, Australia, *Journal of Coastal Research*, *Special Issue 75*, 1297-1301.

Palinkas, C. M., and K. A. Engelhardt (2019), Influence of inundation and suspended-sediment concentrations on spatiotemporal sedimentation patterns in a tidal freshwater marsh, *Wetlands*, *39*(3), 507-520.

Pontee, N. (2013), Defining coastal squeeze: A discussion, *Ocean & Coastal Management*, *84*, 204-207, doi:10.1016/j.ocecoaman.2013.07.010.

Quisthoudt, K., N. Schmitz, C. Randin, F. Dahdouh-Guebas, E. R. Robert, and N. Koedam (2012), Temperature variation among mangrove latitudinal range limits worldwide, *Trees*, *26*(6), 1919-1931, doi:10.1007/s00468-012-0760-1.

Rodríguez, J. F., P. M. Saco, S. Sandi, N. Saintilan, and G. Riccardi (2017), Potential increase in coastal wetland vulnerability to sea-level rise suggested by considering hydrodynamic attenuation effects, *Nature communications*, *8*(1), 1-12.

Rogers, K., et al. (2019a), Wetland carbon storage controlled by millennialscale variation in relative sea-level rise, *Nature*, *567*, 91-95, doi:10.1038/s41586-019-0951-7.

Rogers, K., L. A. Mogensen, P. Davies, J. Kelleway, N. Saintilan, and G. Withycombe (2019b), Impacts and adaptation options for estuarine vegetation in a large city, *Landscape and Urban Planning*, *182*, 1-11, doi:https://doi.org/10.1016/j.landurbplan.2018.09.022.

Rogers, K., and N. Saintilan (2021), Processes Influencing Autocompaction Modulate Coastal Wetland Surface Elevation Adjustment With Sea-Level Rise, *Frontiers in Marine Science*, *8*, 879.

Rogers, K., N. Saintilan, and H. Heijnis (2005), Mangrove encroachment of salt marsh in Western Port Bay, Victoria: The role of sedimentation, subsidence and sea level rise, *Estuaries*, *28*(4), 551-559.

Rogers, K., A. Zawadzki, L. A. Mogensen, and N. Saintilan (2022), Coastal Wetland Surface Elevation Change Is Dynamically Related to Accommodation Space and Influenced by

Sedimentation and Sea-Level Rise Over Decadal Timescales, *Frontiers in Marine Science*, *9*, doi:10.3389/fmars.2022.807588.

Saintilan, N. (2009), Biogeography of Australian saltmarsh plants, *Austral Ecology*, *34*(8), 929-937, doi:10.1111/j.1442-9993.2009.02001.x.

Saintilan, N., N. Khan, E. Ashe, J. Kelleway, K. Rogers, C. D. Woodroffe, and B. Horton (2020), Thresholds of mangrove survival under rapid sea level rise, *Science*, *368*(6495), 1118-1121.

Saintilan, N., K. E. Kovalenko, G. Guntenspergen, K. Rogers, J. C. Lynch, D. R. Cahoon, C. E. Lovelock, D. A. Friess, E. Ashe, and K. W. Krauss (2022), Constraints on the adjustment of tidal marshes to accelerating sea level rise, *Science*, *377*(6605), 523-527.

Saintilan, N., N. C. Wilson, K. Rogers, A. Rajkaran, and K. W. Krauss (2014), Mangrove expansion and salt marsh decline at mangrove poleward limits, *Global Change Biology*, *20*, 147-157, doi:10.1111/gcb.12341.

Sandi, S., J. Rodriguez, P. Saco, N. Saintilan, and G. Riccardi (2021), Accelerated Sea-Level Rise Limits Vegetation Capacity to Sequester Soil Carbon in Coastal Wetlands: A Study Case in Southeastern Australia, *Earths Future*, *9*(9), e2020EF001901.

Schile, L. M., J. C. Callaway, J. T. Morris, D. Stralberg, V. T. Parker, and M. Kelly (2014), Modeling tidal marsh distribution with sea-level rise: evaluating the role of vegetation, sediment, and upland habitat in marsh resiliency, *PLoS ONE*, *9*(2), e88760.

Schuerch, M., T. Spencer, S. Temmerman, M. L. Kirwan, C. Wolff, D. Lincke, C. J. McOwen, M. D. Pickering, R. Reef, and A. T. Vafeidis (2018), Future response of global coastal wetlands to sea-level rise, *Nature*, *561*(7722), 231, doi:10.1038/s41586-018-0476-5.

Sloss, C. R., C. V. Murray-Wallace, and B. G. Jones (2007), Holocene sea-level change on the southeast coast of Australia: a review, *Holocene*, *17*(7), 999-1014.

Sutton-Grier, A. E., A. K. Moore, P. C. Wiley, and P. E. T. Edwards (2014), Incorporating ecosystem services into the implementation of existing U.S. natural resource management regulations: Operationalizing carbon sequestration and storage, *Marine Policy*, *43*(0), 246-253, doi:http://dx.doi.org/10.1016/j.marpol.2013.06.003.

Swanson, K. M., J. Z. Drexler, D. H. Schoellhamer, K. M. Thorne, M. L. Casazza, C. T. Overton, J. C. Callaway, and J. Y. Takekawa (2014), Wetland accretion rate model of ecosystem resilience (WARMER) and its application to habitat sustainability for endangered species in the San Francisco estuary, *Estuaries and Coasts*, *37*(2), 476-492.

Thom, B. G., I. Eliot, M. Eliot, N. Harvey, D. Rissik, C. Sharples, A. D. Short, and C. D. Woodroffe (2018), National sediment compartment framework for Australian coastal management, *Ocean & Coastal Management*, *154*, 103-120.

Thorne, K., G. MacDonald, G. Guntenspergen, R. Ambrose, K. Buffington, B. Dugger, C. Freeman, C. Janousek, L. Brown, and J. Rosencranz (2018), US Pacific coastal wetland resilience and vulnerability to sea-level rise, *Science Advances*, *4*(2), eaao3270.

Torio, D. D., and G. L. Chmura (2013), Assessing Coastal Squeeze of Tidal Wetlands, *Journal of Coastal Research*, *29*(5), 1049-1061, doi:10.2112/jcoastres-d-12-00162.1.

Water Technology (2014), Western Port Local Coastal Hazard Assessment: Report 05 (R05) – Erosion Hazards*Rep.*, 79 pp, Melbourne Water, Melbourne.

White, N. J., et al. (2014), Australian sea levels—Trends, regional variability and influencing factors, *Earth-Science Reviews*, *136*(0), 155-174, doi:http://dx.doi.org/10.1016/j.earscirev.2014.05.011.

Whitt, A. A., R. Coleman, C. E. Lovelock, C. Gillies, D. Ierodiaconou, M. Liyanapathirana, and P. I. Macreadie (2020), March of the mangroves: Drivers of encroachment into southern temperate saltmarsh, *Estuarine, Coastal and Shelf Science*, *240*, 106776.

Wiberg, P. L., S. Fagherazzi, and M. L. Kirwan (2020), Improving predictions of salt marsh evolution through better integration of data and models, *Annual review of marine science*, *12*, 389-413.

Woodroffe, C. D., K. Rogers, K. L. McKee, C. E. Lovelock, I. Mendelssohn, and N. Saintilan (2016), Mangrove sedimentation and response to relative sea-level rise, *Annual Review of Marine Science*, *8*, 243-266.

Zhang, Y., J. C. Rowland, C. Xu, P. J. Wolfram, D. Svyatsky, J. D. Moulton, Z. Cao, M. Marani, A. D'Alpaos, and D. Pasqualini (2020), Understanding the Eco-Geomorphologic Feedback of Coastal Marsh Under Sea Level Rise: Vegetation Dynamic Representations, Processes Interaction, and Parametric Sensitivity, *Journal of Geophysical Research: Earth Surface*, *125*(11), e2020JF005729.

Figure 1. Study location at Westernport Bay, Victoria, Australia, and sub-sites used for model parameterisation, including French Island, Kooweerup, Quail Island and Rhyll Inlet.

Figure 2. Comparisons for SET observations and model simulations in the mangrove and saltmarsh at a) French Island, b) Kooweerup, c) Quail Island, and d) Rhyll Inlet. Mangrove and saltmarsh SET measurements indicated by closed circles and open circles respectively; mangrove and saltmarsh simulations indicated by solid and dashed lines, respectively.

Figure 3. Simulated elevation change between 1974 and 2009 for the seaward and landward mangrove boundaries at a) French Island, b) Kooweerup, c) Quail Island, and d) Rhyll Inlet. Mangrove and saltmarsh simulations indicated by solid lines and dashed lines, respectively.

Figure 4. Substrate profile, and mean elevation and slope of the saltmarsh at a) French Island, b) Kooweerup, c) Quail Island and d) Rhyll Inlet.

Table 1. Matched pairs t-test statistics comparing model simulations (m AHD) to SET measurements (M AHD)at each subsite. * denotes significant differences at significance level of 0.05; † denotes zones within sub-sites where the mean difference in SET measurements and simulations exceeded the mean standard error of SET measurements.

Table 2. Estimated tidal position of the seaward and landward mangrove boundary at each sub-site, hindcast elevation (m) of each boundary at 1974, modelled elevation of each boundary at 2009, expected elevation of each boundary at 2009 based on extraction from a LiDAR-derived digital elevation model, and difference between expected and modelled elevation.

Table 3. Modelled equilibrium elevations at 1900, modelled elevations of the former equilibrium elevation at 2009 and expected elevation at 2009, as per Figure 4 and based on extraction from a LiDAR-derived DEM.

Figure 1.

Service Layer Credits: Source: Esri, Maxar, Earthstar Geographics, and the GIS User Community

Figure 2.

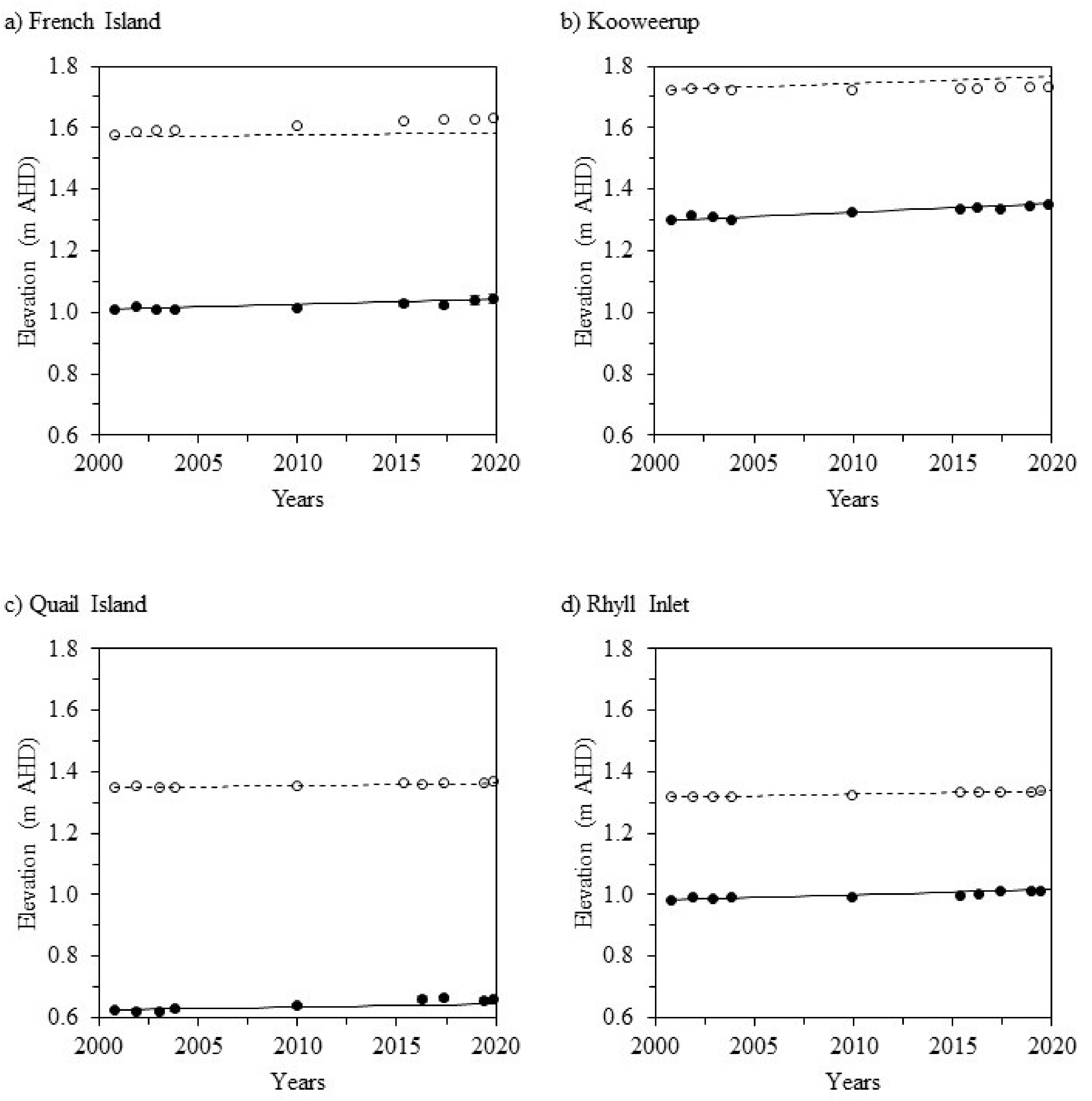

a) French Island
b) Kooweerup
c) Quail Island
d) Rhyll Inlet
Elevation (m AHD)
1.8
1.6
1.4
1.2
1.0
0.8
0.6
2000
2005
2010
2015
2020
Years

Figure 3.

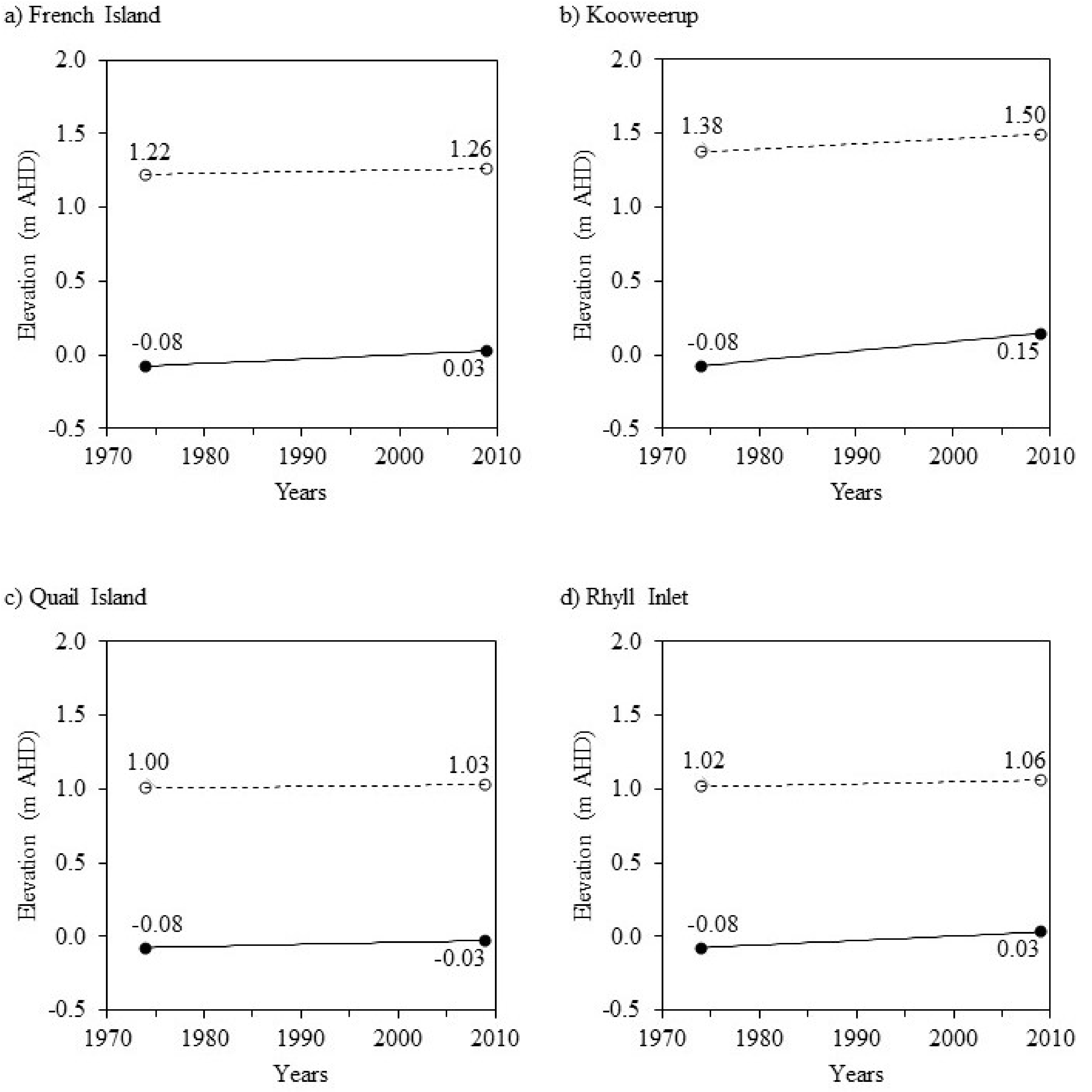
a) French Island
b) Kooweerup
c) Quail Island
d) Rhyll Inlet
Elevation (m AHD)
Years
1.22
1.26
-0.08
0.03
1.38
1.50
-0.08
0.15
1.00
1.03
-0.08
-0.03
1.02
1.06
-0.08
0.03
2.0
1.5
1.0
0.5
0.0
-0.5
1970
1980
1990
2000
2010

Figure 4.

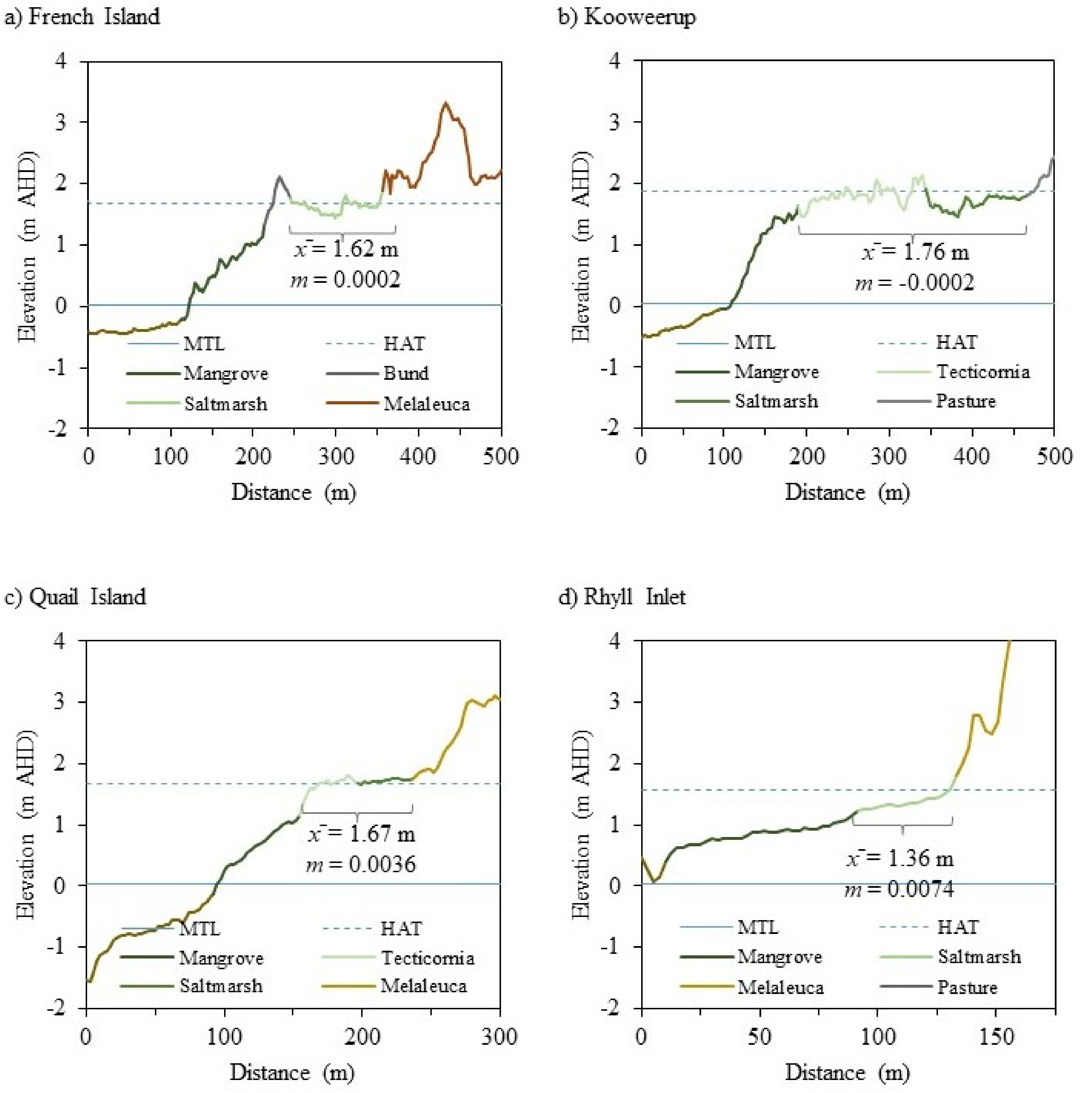

a) French Island
Elevation (m AHD)
Distance (m)
x̄ = 1.62 m
m = 0.0002
MTL
HAT
Mangrove
Bund
Saltmarsh
Melaleuca
b) Kooweerup
Elevation (m AHD)
Distance (m)
x̄ = 1.76 m
m = -0.0002
MTL
HAT
Mangrove
Tecticornia
Saltmarsh
Pasture
c) Quail Island
Elevation (m AHD)
Distance (m)
x̄ = 1.67 m
m = 0.0036
MTL
HAT
Mangrove
Tecticornia
Saltmarsh
Melaleuca
d) Rhyll Inlet
Elevation (m AHD)
Distance (m)
x̄ = 1.36 m
m = 0.0074
MTL
HAT
Mangrove
Saltmarsh
Melaleuca
Pasture